Plasma Expansion and Evolution of Density Perturbations in the Polar Wind: Comparison of Semikinetic and Transport Models

C. W. Ho, J. L. Horwitz, N. Singh and G. R. Wilson

Department of Physics and Center for Space Plasma and Aeronomic Research, The University of Alabama in Huntsville

Comparisons are made between transport and semikinetic models in a study of the time evolution of plasma density perturbations in the polar wind. The situations modeled include plasma expansion into a low-density region and time evolution of localized density enhancements and cavities. The results show that the semikinetic model generally yields smoother profiles in density, drift velocity, and ion temperature than the transport model, principally because of ion velocity dispersion. While shocks frequently develop in the results of the transport model, they do not occur in the semikinetic results. In addition, in the semikinetic results, two ion streams, or double-humped distributions, frequently develop. In the transport model results the bulk parameters, at a given time, often have a one-to-one correspondence in the locations of their local minima or maxima. This is a consequence of the coupling of the fluid equations. There is, however, no such relationship among the moments produced by the semikinetic model where the local moment maxima and minima are often shifted in altitude. In general, incorporation of enhanced heat fluxes in the transport model leads to somewhat improved agreement with the semikinetic results.

Introduction

Numerous models have been developed in the last three decades to treat the outflow of plasma from the topside ionosphere. These models fall mainly into two categories: kinetic descriptions and hydrodynamic descriptions. Hydrodynamic models were first formulated by *Banks and Holzer* [1968]. In assuming an isothermal temperature distribution, they found that the electric field, which is determined by the electron pressure gradient, is strong enough to accelerate H^+ and He^+ ions to supersonic velocities. This and other related studies [*Banks and Holzer*, 1969; *Marubashi*, 1970] established the basic characteristics of the polar wind, such as the ion density versus altitude and the outflow fluxes.

Realizing that ions become collisionless and their velocity distributions highly anisotropic at sufficiently large radial distances, *Dessler and Cloutier* [1969] proposed a single-particle evaporative polar "breeze" model as an alternative to the hydrodynamic approach. They argued that ion acceleration due to the polarization electric field occurs at altitudes where the mean free path is large, and where the ions cannot be regarded as interacting directly with each other. They questioned the pressure gradient term in the hydrodynamic equations of motion and argued that it cannot be responsible for the acceleration of the light ions. This led to the famous Banks-Holzer and Dessler-Cloutier controversy which is discussed in detail by *Donahue* [1971].

Since the early theoretical models of the polar wind were established in the late 1960s and early 1970s [*Banks and Holzer*, 1968; 1969; *Holzer et al.*, 1971; *Lemaire and Scherer*, 1970; 1971], polar outflows have been studied through the use the hydrodynamic or transport [*Schunk and Watkins*, 1981; *Mitchell and*

Palmadesso, 1983; *Singh and Schunk*, 1985; 1986; *Ganguli and Palmadesso*, 1987; *Ganguli et al.*, 1987; *Gombosi and Nagy*, 1988], ion kinetic [*Horwitz and Lockwood*, 1985; *Horwitz*, 1987] and semikinetic [*Barakat and Schunk*, 1983; *Li et al.*, 1988; *Wilson et al.*, 1990; *Brown et al.*, 1991; *Ho et al.*, 1992] models.

Transport models involve the solution of a set of N moment equations solving for $N + 1$ bulk parameters. The equation set is closed by expressing the highest moment as an assumed function of the lower order moments. The principal advantages of the transport model include its efficiency in the use of computer resources (compared to the semikinetic model) and its ability to easily include chemical and collisional processes. However, many problems require a detailed knowledge of the ion velocity distribution function beyond that which would be available from a transport model. The ability of a transport model to accurately describe the velocity distribution increases with the order of the moment equations employed, but the highest order equations can be difficult to solve [e.g., *Gombosi and Rasmussen*, 1991]. In contrast, in solving the Boltzmann equation the kinetic model solves an infinite hierarchy of moment equations since its results yield the full distribution function. This however is achieved at the expense of computer efficiency. As an approximate solution to the Boltzmann equation one can solve the gyro-averaged Boltzmann equation by a hybrid or semikinetic (kinetic ions, fluid electrons) technique.

In view of the vastly different formulations of the kinetic and hydrodynamic models applied to the same geophysical environments by different investigators over the past two decades, it is necessary to compare the two approaches in such a way so as to elucidate the differences, applicability, and limitations of the two approaches. Except for some limited work done in the early 70's by *Holzer et al.* [1971] and *Lemaire and Scherer* [1972], recently only *Demars and Schunk* [1992] have compared the semikinetic with the transport models for the steady state polar wind. Their results showed close agreement in the density, drift velocity, parallel and perpendicular temperatures, and parallel and perpendicular heat flows from both models. They concluded that the bi-Maxwellian based transport equations are an appropriate tool for studying space plasmas that develop non-Maxwellian features. However, good agreement between the steady state solutions from the two models does not necessarily mean that they will continue to agree when time evolving problems are considered.

The purpose of the present study is twofold. First, and foremost, is to investigate the appropriateness of using the transport model for dynamic situations, especially in the collisionless domain. This part of the study is accomplished by direct comparison of the moments produced by a transport and a semikinetic model. Of particular interest is the question of whether steep gradient persistence (i.e., shocks) are unique to

the transport model. Another question involves the consequences of phase mixing [*Palmadesso et al.*, 1988] which is disallowed in the transport model because of the truncation of the moment hierarchy but is naturally included in the semikinetic model. Phase mixing can be responsible for damping thermal waves. By analyzing the degree of agreement of transport with semikinetic models, we can assess the appropriateness of using such transport models in global systems, where semikinetic modeling is currently not feasible. The second purpose of this study is to extend the work of *Singh and Schunk* [1985] on the study of the time evolution of density perturbations in the polar wind. In the present study a more sophisticated transport model and a semikinetic model are used to study the same situations considered by Singh and Schunk.

Semikinetic Model

The semikinetic model used in this paper is the same as that developed by *Wilson et al.* [1990]. The model is based on a hybrid particle-in-cell approach which treats the ions (H^+) as parallel-drifting gyrocenters injected, at the lower boundary, as the upgoing portions of a drifting bi-Maxwellian distribution. The electrons are treated as a massless neutralizing fluid.

We simulate the motion of H^+ in a magnetic flux tube extending from 1.47 to 10 R_E. Within this altitude range the plasma is taken to be collisionless. The ions at the exobase (1.47 R_E) are assumed to be bi-Maxwellian and the upgoing ions of these distributions are injected into the simulation region. The distribution function used for injecting new ions at the base of the flux tube is given by

$$f_o(v_\parallel \geq 0) = n_o \frac{(m/2\pi k)^{3/2}}{T_{\perp o}\sqrt{T_{\parallel o}}} \cdot \exp\left(-\frac{m(v_\parallel - u_o)^2}{2kT_{\parallel o}} - \frac{mv_\perp^2}{2kT_{\perp o}}\right) \quad (1)$$

$$f_o(v_\parallel < 0) = 0$$

where the subscripts o represents the various parameters of the injected ions at the base of the flux tube, $v_\parallel$ and $v_\perp$ are the parallel and perpendicular velocities, m is the ion mass and k is Boltzmann's constant. For this study, we use the polar wind parameters similar to *Singh and Schunk* [1985] for the injected H^+ distribution functions: an upgoing drift speed (u_o) of 20 km/s; a density (n_o) of 500 ions/cm^3; and parallel and perpendicular temperatures ($T_{\parallel o}$, $T_{\perp o}$) of 3560 K.

The parallel force along the magnetic field line acting on the ions is

$$F_\parallel = mg_\parallel + q_i E_\parallel - \mu \nabla B \quad (2)$$

where q_i is the charge of the ion, $g_\parallel$ is the gravitational acceleration which varies as $1/r^2$, μ ($= \frac{1}{2}mv_\perp^2/B$) is

the ion's magnetic moment, and $E_\parallel$ is the polarization electric field parallel to the magnetic field, B. B is assumed to vary as r^{-3}. The term $-\mu\nabla B$ is the magnetic gradient or magnetic mirror force. The assumed constancy of μ determines the perpendicular speed $v_\perp$.

By assuming that the electrons are isothermal and have zero mass, the electric field is given by the Boltzmann relation

$$E_\parallel = -\frac{kT_e}{n_e e}\frac{dn_e}{dr} \tag{3}$$

where k and e are the Boltzmann constant and the magnitude of the electronic charge, T_e is the electron temperature taken to be the same as the ion temperature at r_o, and n_e is the electron density which is assumed to be equal to the ion density.

Transport Model

The collisionless transport equations governing the magnetic field aligned gyrotropic motion of ions are the equations of continuity, momentum and parallel and perpendicular thermal energy given by the following:

$$\frac{\partial n}{\partial t} + \frac{\partial}{\partial s}(nv) = \frac{-nv}{A}\frac{\partial A}{\partial s} \tag{4}$$

$$\frac{\partial v}{\partial t} + \frac{\partial}{\partial s}(\frac{1}{2}v^2) = (\frac{q_i}{m})E_\parallel - (\frac{k}{m})\frac{\partial T_\parallel}{\partial s} - (\frac{k}{m})T_\parallel\frac{1}{n}\frac{\partial n}{\partial s} - g_\parallel(r) - (\frac{k}{m})(T_\parallel - T_\perp)\frac{1}{A}\frac{\partial A}{\partial s} \tag{5}$$

$$\frac{\partial T_\parallel}{\partial t} + \frac{\partial}{\partial s}(vT_\parallel) = -T_\parallel\frac{\partial v}{\partial s} - \frac{1}{nA}\frac{\partial}{\partial s}(q_\parallel A) + 2q_\perp\frac{1}{nA}\frac{\partial A}{\partial s} \tag{6}$$

$$\frac{\partial T_\perp}{\partial t} + \frac{\partial}{\partial s}(vT_\perp) = T_\perp\frac{\partial v}{\partial s} - T_\perp v\frac{1}{A}\frac{\partial A}{\partial s} - \frac{1}{nA}\frac{\partial}{\partial s}(q_\perp A) - q_\perp\frac{1}{nA}\frac{\partial A}{\partial s} \tag{7}$$

where t is time; r is the geocentric distance to the point along the flux tube, s is the distance along the tube from its lower boundary, $n, v, T_\parallel$, $T_\perp$, $q_\parallel$ and $q_\perp$ are the number density, flow velocity, parallel and perpendicular temperatures and heat flows of the polar wind ions, respectively. $E_\parallel$ is the parallel electric field (found from equation (3)), $g_\parallel$ is the component of the gravitational force parallel to the magnetic field, m, q_i and k are the ion mass, ion charge and Boltzmann constant, respectively. A is the cross-sectional area of a flux tube ($A \propto r^3$).

This set of differential equations is solved numerically by the flux-corrected transport technique [*Boris and*

Book, 1976] and are closed by using heuristic expressions for the heat flow $q_{\parallel}$ and $q_{\perp}$, which closely follow the treatments in the solar wind studies [*Metzler et al.*, 1979]. In a collisionless plasma, the usual expression for heat flow, given by $q_\alpha = -K_\alpha \nabla T_\alpha$ with K_α (where α denotes $\parallel$ or $\perp$) as the thermal conductivity may not be valid because the mean free path $\lambda \gg (T^{-1}\partial T/\partial s)^{-1}$. In such a situation the maximum heat flow may be given by the transport of thermal energy (nkT_α) by the unidirection parallel thermal velocity $v_{th} = (kT_\parallel/2\pi m)^{\frac{1}{2}}$ [*Palmadesso et al.* 1988]. Accordingly, it can be shown that (N. Singh et al., Comparison of hydrodynamic and semikinetic models for plasma flow along closed field lines, submitted to *Journal of Geophysical Research*, 1993), 1993]

$$q_\alpha = \epsilon \eta_\alpha n k T_\alpha v_{th_\alpha} \tag{8}$$

where $\epsilon = -1$ if $\partial T_\alpha/\partial s > 0$ and $\epsilon = 1$ if $\partial T_\alpha/\partial s < 0$. Thus, the temperature gradient determines the sign of the heat flow but not its magnitude. The factor η_α gives the reduction in heat flow due to anomalous plasma effects. In the present calculations we cannot determine the value of η_α self-consistently. We study the effect of the heat flow on the results by varying the values of η_α. *Gombosi and Rasmussen* [1991] demonstrated that in order to get realistic distribution functions from the 20-moment model, the heat flow must be small compared to the thermal speed times the pressure. In this paper, $\eta_\alpha = 0$ represent no heat flow, while $\eta_\alpha = 1$ corresponds to the theoretical maximum heat flow. However, since (8) is only a heuristic equation, we will take the liberty of using values for η_α larger than unity to study the effect of large heat flow in a later section of this paper. Although the above expression for heat flow is a simplification it allows the inclusion of heat flow in the study rather easily and produces reliable results at least for steady state (Figure 1). As such it is used as a preliminary study before the full heat flow transport equations can be implemented.

Before we compare the results of the two models for the time-dependent cases, we shall first compare the steady state polar wind results. Figure 1 shows the density, drift velocity, parallel and perpendicular (to the direction of the magnetic field) temperatures, and parallel and perpendicular heat flows of the steady state polar wind solutions with boundary conditions given in the last section. The results of the two models show good agreement in general. The drift velocity obtained from the transport model (solid curve) is higher than that of the semikinetic model. This discrepancy also appears later when we show the time evolution of the drift velocity. The reader should keep this in mind in subsequent comparisons.

The density, drift velocity, and perpendicular temperature of the transport model results are little affected by the choice of the heat flow parameter η_α in

equation (8). However, both a higher parallel and perpendicular heat flow increase the parallel temperature. We found that a value of 0.3 for both $\eta_{\parallel}$ and $\eta_{\perp}$ gives the closest agreement between the parallel temperature profiles of the two models. In a later section of this paper, we shall discuss in more detail the effects, on the various moments, of varying the parallel and perpendicular heat flows in a time-dependent situation.

With our particular choice of the amount of heat flow ($\eta_{\parallel} = \eta_{\perp} = 0.3$), there is a cross-over at 5.5 R_E for the parallel heat flow profiles from the two models. Below the cross-over the parallel heat flow in the transport model is higher than that of the semikinetic model. Both the parallel and perpendicular heat flows obtained from the semikinetic model increase sharply near the lower boundary, and then decrease with altitude above 1.7 R_E. The transport model used in this particular paper failed to produce this feature. *Demars and Schunk* [1992] used a 16-moment transport model which produced a sharp bend in the heat flow profiles at low altitude. This could be due to the inclusion of collisions in their transport model and/or their use of the full heat flow equation to solve for $q_{\parallel}$ and $q_{\perp}$. Their semikinetic model did not produce the low altitude heat flow bend when they assumed a Maxwellian velocity distribution at the boundary, but it did when the distribution was a bi-Maxwellian with zero stress. It should be noted that *Demars and Schunk* [1992] compared the steady state polar wind model to about 2.9 R_E while a flux tube extending to 10 R_E is used in this paper.

Expansion of the Polar Wind into a Low Density Plasma

Satellite observations indicate that the ions in the magnetosphere of ionospheric origin are much more energetic than those in the ionosphere [*Baugher et al.*, 1980; *Horwitz and Chappell*, 1979]. The energization of these ionospheric ions can be explained in terms of various mechanisms, one of which is connected with the outward expansion of the topside, high-latitude ionospheric plasma along open geomagnetic field lines [*Singh and Schunk*, 1982, 1986]. In this section we study the time evolution of the polar wind expanding into a low density region. The study will be conducted using both the semikinetic and transport models described earlier. Our initial conditions are the same as used by *Singh and Schunk* [1985], who assumed a sudden drop of plasma density above a certain altitude. Note that the initial conditions we used here (and subsequent sections) may not represent real physical situations. We are mainly interested in the comparison of the results of two different models under the same conditions. Our results, however, are important to the study of the time evolution of density perturbations in space plasmas in general, irrespective of the initial boundary conditions.

At time $t = 0$, the density of the steady state polar wind was lowered to 0.5 ions/cm^3 at and above an altitude of 9000 km (density profile t_0, Figure 2*a*). The plasma was then allowed to evolve in time using both the semikinetic and transport models. Bulk parameters were calculated from the ion distribution function in the semikinetic model at the same selected times at which bulk parameters from the transport model were output. The transport model used for its initial conditions bulk parameters obtained from the semikinetic model at t_0. Profiles of the density, drift velocity and parallel temperature, at different times, from both the semikinetic (dotted curves) and transport (solid curves) models are shown in Figure 2. The profiles in Figure 2 are separated by a time of 5 min.

The density profiles from both models can generally be broken down into three regions, which are indicated by *a*, *b* and *c* on profile t_1. Region *a* ($r < 3$ R_E) is the unperturbed polar wind solution, region *b* (3 - 4.5 R_E) is the polar wind expansion into a region of low density plasma, and region *c* ($r > 4.5$ R_E) is the region of low density plasma still flowing upwards. Region *a* expands in altitude range as time advances because the polar wind is being continuously supplied from below the lower boundary. The perturbation propagates upward while the density profile returns to the steady state solution. As the plasma in the low density region (region *c*) moves upward its density decreases because of the divergence of the flux tube. In a 15-min period the density at the upper boundary drops by about half. In region *c* the bulk drift velocity also decreases slightly from the steady state value because the electric field goes from being zero to being slightly negative because of the positive density gradient.

To understand the region of plasma expansion (region *b*), it is helpful to examine the ion distribution function. Figure 3 shows the reduced distribution function which is the ion distribution integrated over all perpendicular velocities and plotted in a phase space of parallel velocity versus radial distance. This distribution is displayed in a gray-scale format such that darker shades represent higher density. At $t = 0$, the electric field at the high/low-density boundary is very large because it is proportional to the initial large gradient of the density. This electric field accelerates ions in both the high- and low- density regions immediately adjacent to the density interface. These ions flow upwards and disperse in time. As they do, the density gradient and the large associated electric field diminish. Also, the dispersing ions produce a region of elevated parallel velocity, and a region where the parallel temperature is first reduced below and then elevated above the steady state temperature profile. The region of elevated drift speed is simply a result of the many high speed particles from below overtaking the slower ions above them. The region of temperature reduction occurs where ions are cooled by acceleration through the large interface potential drop. The region

of temperature enhancement develops where two ion streams exist. The altitudinal extent of each of these regions expands in time because of velocity dispersion.

The transport model results are very similar to the semikinetic model results in region *a* and *c*, but there are significant differences in the transition region *b*. A sharp and persistent density jump develops at the upper edge of this region. At the same location there is an abrupt jump in the drift velocity and parallel temperature. This shock propagates upwards with a speed of about 38 km/s which is consistent with the Rankine-Hugoniot relation [*Singh and Schunk*, 1985]. As this shock moves upward a local density minimum develops below it. This region of minimum density—where the maximum drift velocity and parallel temperature occur—behind a forward shock is a reverse shock [*Sonett and Colburn*, 1965]. Nothing corresponding to these features are seen in the semikinetic bulk parameter profiles. They are smooth and continuous throughout this region.

The parallel ion temperature obtained from the transport model also has a leading elevated value and a trailing suppressed value; however, this wave feature moves up the flux tube more slowly than the similar feature seen in the semikinetic temperature results. Velocity dispersion plays an important role in creating this difference. The first ions to reach a given altitude are ions with high velocity. When they first arrive, however, they make up only a small fraction of the total number of ions present. Their contribution to the local bulk moments become more pronounced as their velocity, raised to increasing powers, starts to outweigh their small relative numbers. One would then expect to see increasing disagreement among transport and semikinetic model moments with increasing moment order, to the degree to which the transport model does not properly describe the effects of velocity dispersion. In the case under discussion here, the disagreement is quite pronounced starting at the parallel temperature moment.

The shock in the results of the transport model in Figure 2 can be seen as discontinuous jumps in the density, drift velocity, and parallel temperature. Clearly, the values of all three of these moments are tightly coupled at the location of the shock. In figure 4*a* one can see the density, drift speed and parallel temperature profiles from the transport model at $t = 15$ min. In addition to the correlation among the moments evident at the shock, other instances of correlation (such as the point where the maximum drift speed and parallel temperature occur) can be seen. This correlation is, of course, a consequence of the coupled nature of the differential equations in the transport model. The semikinetic model results display no such correlation among the moments as can be seen in the profiles in figure 4*b*. This is a consequence of phase mixing where kinetic effects damp waves generated by the initial perturbation. In

the transport model such waves persist because the truncated moment set does not allow phase mixing.

The temperature elevation of the semikinetic model (e.g., between 7 and 10 R_E at $t = 15$ min in Figure 2c) is the "effective temperature" that results when the ions in the low density region and the ions in the high speed stream are counted as one population. Such "effective temperature" is not found in the transport results when only one ion stream is simulated. Multistream fluid codes can be implemented for streams originating from specified sources, however, such codes cannot model plasmas which develop multiple streams during the course of the simulation, unless the locations and times where such streams will develop can be anticipated.

Like the density profile, parallel heat flow (parallel thermal energy per unit area per unit time) shows a sudden drop at about 2.4 R_E at $t = 0$ when the perturbation is first imposed (not shown). However, the parallel and perpendicular heat flow per ion retain the same profile at $t = 0$ as that of the steady state polar wind because the distribution function remains exactly the same as the steady state polar wind at $t = 0$ except for a uniform number density above 2.4 R_E. (In the following we shall restrict our discussion to the heat flow per ion as it is found to be more illuminating.) Figure 5 shows the parallel heat flow per ion at time $t = 15$ min. The semikinetic profile (dotted curve) has a negative heat flow from about 6.2 to 8.1 R_E which corresponds to the positive slope of the parallel temperature as seen in Figure 4b. It also has positive heat flow above and below this region where the parallel temperature has a negative slope. One can see from this that the semikinetic results support the idea that the sign of the heat flow depends on the sign of the slope of the temperature, as used in the transport model formulation (Equation (8)).

The parallel heat flow calculated from the transport model (solid curve) also has a local minimum and maximum around 7.4 R_E. The direction of the heat flow is determined by the slope of the parallel temperature as required by (8). The magnitude of the local minimum and maximum heat flow is about an order of magnitude less than that obtained from the semikinetic model. An increase of η_α in (8) will make the comparison of the heat flow of the two models more favorable. Later on, we shall see that a larger heat flow will result in a better agreement of the lower moments also. The reader should bear in mind that the value of η_α use here ($\eta_\alpha = 0.3$) was chosen so that the steady state solutions of both models would be as close as possible. The effect of varying η_α on the transport model results, will be discussed later.

Evolution of a Localized Density Enhancement

The Earth-space environment is a region of dynamic plasma phenomena. Both heavy and light ions are created and destroyed through photoionization and

charge exchange in the ionosphere, and are continuously transported throughout the magnetosphere. One should therefore expect to find regions in the magnetosphere where the plasma densities are high and regions of relatively low density. For instance, density enhancements at high altitude could arise from electric field heating at low altitudes [*Hultqvist*, 1991] followed by the upward propagation of the hot plasma to higher altitudes. Recently *Singh* [1992] has shown that plasma enhancements and cavities can be created by transverse ion heating via wave-particle interactions. In this section, we will investigate the time evolution of a localized plasma density enhancement in the classical supersonic H^+ polar wind.

The density of the imposed plasma enhancement is given at time $t = 0$ by

$$n_{enh}(r) = p n_{pw}(r) e^{-\frac{1}{2}(\frac{r-r_p}{\sigma})^2} \qquad (9)$$

where $n_{pw}(r)$ is the steady state polar wind density. $n_{enh}(r)$ is therefore a Gaussian distribution along r with a peak value of p times n_{pw} at $r = r_p$. We chose p, σ and r_p to be 5, 1260 km and 15600 km respectively. The plasma density enhancement has zero flow velocity initially and has an ion temperature of 500 K for both $T_\parallel$ and $T_\perp$.

The density, flow velocity and parallel temperature of the semikinetic model at $t = 0$, when the density enhancement was first introduced, are given in Figures 6*a*, 6*b* and 6*c* and are marked by t_0 (Dotted curve). Again, the plasma distribution function in parallel velocity and radial distance phase space, as shown in Figure 7, are used to interpret the various bulk parameters. The stationary plasma density enhancement causes the net bulk velocity to decrease to about 4 km/s at the peak of the density enhancement, compared to 23 km/s for the steady state polar wind (dashed curves). The double peak in the parallel temperature profile at $t = 0$ can be explained in the following way. When nearly equal populations with a relative drift exist, the parallel temperature will be associated with the separation, in velocity space, of these populations. When either population is dominant, the temperature will be approximately that of the dominant population. At 2 and 2.8 R_E the density of the imposed plasma population is comparable to that of the polar wind. At the center of the imposed population, at 2.4 R_E, the imposed ion density exceeds the polar wind background density. Where these two different populations have near equal numbers the effective temperature is the highest. At points where one dominates the other the effective temperature tends toward that of the dominant population.

The density profiles obtained by the semikinetic model (dotted curves, Figure 6*a*) show that the density enhancement flattens out with time. This is due in large part to the distribution of ion velocities (both positive and negative) in the density enhancement. This

dispersional flattening of the density enhancement can be seen in the phase plot in Figure 7*b* where the density enhancement is now very elongated. The electric field modifies the dispersion of the enhancement because above and below the density peak it has opposite signs (as a result of opposite density gradients). Above the peak it is positive and accelerates the ions upward, while below the peak it is negative and accelerates the ions downward. The downward flowing ions increase the density of the plasma at the lower boundary, and lower somewhat the flow velocity of the plasma.

In comparing with the results of the semikinetic model in a consistent manner, one could use in the transport model the same initial bulk parameter profiles as produced by the semikinetic model. However, in a single-fluid treatment, the initial parallel temperature profile of the semikinetic model would be interpreted as a warm density enhancement. In order to find out how a cold density enhancement would evolve under a hydrodynamic treatment, we use the transport model with initial conditions established by the usual definitions for a single fluid:

$$\bar{v} = \frac{n_0 v_0 + n_1 v_1}{n_0 + n_1} \tag{10}$$

$$\bar{T}_\alpha = \frac{n_0 T_{\alpha 0} + n_1 T_{\alpha 1}}{n_0 + n_1} \tag{11}$$

where $\bar{v}$ and $\bar{T}_\alpha$ are the average flow velocity and ion temperature and α stands for $\parallel$ or $\perp$. The "0" subscript denotes the polar wind while the "1" subscript indicates parameters of the density enhancement. In (10) and (11), $n_1 = n_{enh} - n_{pw}$, $v_1 = 0$ and $T_{\alpha 1} = 500$ K. These initial profiles are shown in Figure 6 (solid curve, $t = 0$). The velocity profile at $t = 0$ obtained from (10) is very close to the semikinetic model initial profile, however, the parallel temperature profile at $t = 0$ has a minimum value at the peak of the density enhancement which indicates that the density enhancement is cold.

It is necessary to point out that the discrepancies of the two models at the lower boundary are due to the difference between the way the boundary conditions are handled in each case. In the transport model the density, the drift speed, and the parallel and perpendicular temperatures have specified unchanging values at the lower boundary. In the semikinetic model only the distribution of upgoing ions at the lower boundary is held fixed. The velocity distribution of downgoing ions at the lower boundary is determined by what happens in the flux tube, and as a result, will change with time. The moments found from integrations over the total velocity distribution (upgoing and downgoing ions) will also change. The increase in the density, the drop in the drift speed and the rise in the parallel temperature seen in the semikinetic results at the lower boundary result from part of the ions from the density enhancement population falling out of the base of the flux tube.

In the various transport bulk parameter profiles seen in Figure 6 a number of small scale features develop. The number of these features increases with time. They are also seen to move upward with varying speeds. Although we have not done the wave analysis of the transport model used in this paper, we believe that these features result because of the excitation of several fundamental wave modes by the initial perturbation. (It is likely that these wave modes will be different from those discussed by *Gombosi and Rasmussen* [1991] because of differences between the transport model used in this paper and the 20-moment expansion of Gombosi and Rasmussen.) Differences in the phase velocity of the different modes lead to the development of increasing numbers of small-scale features. If a transport model solving the heat flow equations were used the solution would change no doubt; the old wave modes would be modified and new ones would be introduced. Since the semikinetic results do not develop the same small scale features as are produced by the generalized transport model used in this paper, it is clear that most of these wave modes are spurious. Phase mixing in the semikinetic model is responsible for their elimination.

We have also compared with the semikinetic results, the results from the transport model when its initial parameter profiles are taken to be the same as those produced by the semikinetic model at $t = 0$ [*Ho et al.*, 1993]. Although in this case, an imposed cold plasma (semikinetic) and a warm plasma (transport) are compared, it is interesting to note that the results are closer than the case when a cold plasma enhancement (according to equations (10) and (11)) is used. Furthermore, *Ho et al.* [1993] show that when a strong heat flux was induced artificially by increasing the value of η_4 in (8), the shocks are eliminated and the results of the transport and semikinetic models are much closer.

Evolution of a Localized Density Cavity

In this section, we study the time evolution of a localized density cavity in the steady state H^+ polar wind. The cavity was created by decreasing the density of the plasma along r by

$$n_{cav}(r) = p n_{pw}(r) e^{-\frac{1}{2}\left(\frac{r-r_p}{\sigma}\right)^2} \qquad (12)$$

where $p = 0.9$, σ and r_p have the same meaning and values as in case of the density enhancement (1260 and 15,600 km respectively). The density profile t_0 in Figure 8*a* is therefore given by

$$n(r) = n_{pw} - n_{cav} \qquad (13)$$

where n_{pw} is the density of the steady state polar wind. Since the ion distribution is unchanged, the velocity and parallel temperature at $t = 0$ when the cavity is

created are the same as that of the steady state polar wind (t_0, Figures 8*b* and *c*).

For the semikinetic model, the cavity propagates upward, becomes less deep, and extends over a larger altitude range in time. The cavity propagates with an average speed of about 30 km/s. From the ion distribution function (Figure 9), the cavity is seen to lean towards the abscissa in time. This is again due to velocity dispersion and explains the spreading out of the cavity in time.

The drift velocity and the parallel temperature profiles can also be readily interpreted by inspecting the ion distribution function. For instance, at $t = 15$ min, the reduced number of low-velocity ions near 5 R_E (Figure 9*b*) causes a higher bulk velocity at that altitude, while the loss of ions at the high-velocity end around 7 R_E causes a lower bulk velocity there. The resultant velocity profile is a rounded double-sawtooth structure (Figure 8*b*, dotted curve).

At $t = 15$ min, the parallel velocity distribution function at 4.5 R_E and 7.5 R_E is narrower than at other altitudes which results in lower parallel temperatures there. Note that the locations where the velocity has a local minimum and maximum do not occur at the same altitudes as where the parallel temperature minima occur. (In the transport model results these locations do line up.) Sandwiched between the two low temperature regions is a region of higher temperature (about 1.6 times that of the steady state polar wind) The high temperature is a result of the double-humped distribution formed by the cavity seen in the phase space plot (Figure 9*b*). These structures, in both the velocity and parallel temperature profiles, propagate upward in time and become less sharply defined due to ion dispersion.

The density profiles from the transport model are significantly different. Figure 8*a* (solid curves) show that within 5 min after the local density cavity has been created, the cavity is being filled with ions to form two separate cavities. These cavities propagate upwards with speeds of 22 and 33 km/s, respectively, getting further and further apart. The velocity profiles of the transport model also develop a double saw-tooth structure as in the semikinetic case. However, the velocity enhancement (lower "tooth") and depression (upper "tooth") are separated more and more in time and are linked by a region where the velocity returns to the unperturbed steady state value. It is important to note that the location of the velocity enhancements and depressions correspond to the secondary cavities in the transport model results while for the semikinetic model they correspond to the inner walls of the original cavity. Note also that the overall discrepancy of the velocity profiles of the two models at later time is due to the discrepancy of the two models in flow velocity in steady state (see Figure 1*b*). The time-dependent behavior of a cavity in a plasma obtained by the transport model is similar to the results of *Singh and Schunk* [1985].

Figure 8c compares the parallel temperature of the cavity in the polar wind obtained by both the semikinetic and transport models. In comparison to the semikinetic model, the parallel temperature of the transport model shows the same structure of a high temperature region sandwiched between two low temperature regions. However, the transport model parallel temperature does not spread out as much and the low and high temperature regions remain distinct with magnitudes that decrease with time.

Effect of Heat Flow on the Transport Model Results

The values for $\eta_{\|}$ and $\eta_{\perp}$ used for the heat flow in (8) for all the cases we have studied so far is 0.3. This value gave the best comparison between the semikinetic and transport models at steady state. For steady state, the amount of heat flow was found to have a negligible effect on all of the bulk parameters except the parallel temperature. Figure 10 shows that the exclusion of heat flow in the transport model ($\eta_{\alpha} = 0$) causes the parallel temperature (dotted-dashed curve) to be lower than the semikinetic model (dotted curve) at steady state. We found that both the parallel and perpendicular heat flow can increase the polar wind parallel temperature. When $\eta_{\|} = 1$, $T_{\|}$ (dashed curve) was brought close to the curve of the semikinetic model, while $\eta_{\perp} = 1$ alone yields an even higher $T_{\|}$ (dashed-dotted-dotted-dotted curve). When both $\eta_{\|}$ and $\eta_{\perp}$ equal one the highest $T_{\|}$ (solid curve) results. It is about 500 K higher at the upper boundary than the case without heat flow. The fact that $q_{\perp}$ can affect $T_{\|}$ can be seen from equation (6), in which the last term converts transverse energy to parallel energy by means of the mirror force. In comparison with the $q_{\|}$ term, $q_{\perp}$ has a larger effect on $T_{\|}$ because the term which is dependent on $q_{\|}$ in equation (6) can be broken down into a negative and positive term. The negative term decreases $T_{\|}$ for increasing $q_{\|}$, while the positive term is proportional to $\partial q_{\|}/\partial s$, and has a magnitude smaller than the term which depends on $q_{\perp}$.

Although the amount of heat flow has effects only on the parallel temperature at steady state, we found that it can greatly affect various other bulk parameters in a time-dependent situation. By increasing the heat flow the sharpness of the shocks is reduced and smoother bulk parameter profiles are produced. This can be seen from Figure 11 which shows the density and parallel temperature for different heat flow parameters η_{α}, at a time of 15-min after the density enhancement was imposed on the steady state H^+ polar wind. When $\eta_{\|}$ and $\eta_{\perp}$ both equal 1 the shocks produced by the density enhancement are reduced in comparison to the case when there is no heat flow (dashed curve in comparison to dashed-dotted curve, Figure 11). We have seen from Figure 5 that the heat flow from the semikinetic model can be about an order of magnitude larger than that of the transport model when $\eta_{\|}$ and $\eta_{\perp}$ is taken to be

0.3. By using large values of $\eta_{||}$ and $\eta_{\perp}$ (7.5 for the solid curves in Figure 11), the heat flow obtained from the transport model is increased by 25 times, and the magnitudes of the heat flow from the two models are closer.

In allowing $\eta_{||}$ and $\eta_{\perp}$ to be larger than 1 we have violated the original assumption that the heat flow cannot be larger than the pressure times the thermal speed [*Gombosi and Rasmussen*, 1991]. However, since (8) is only a heuristic formula, there is in practice no limit on the magnitude of $\eta_{||}$ and $\eta_{\perp}$. It is shown in Figure 11 that the sharp gradient structures of the transport model profiles are reduced when increasing values of $\eta_{||}$ and $\eta_{\perp}$ are used. The results obtained by the transport model for large heat flow are closer to those of the semikinetic model. There are situations when the hydrodynamic shocks can be totally dissipated by a large heat flow, this is found in the case of a warm plasma imposed in the polar wind [*Ho et al.*, 1993].

The values of the heat flow parameters $\eta_{||}$ and $\eta_{\perp}$ which were chosen to give a favorable comparison between the transport model and the semikinetic model at steady state have been shown to be too small for a evolving cold plasma density enhancement. This implies that a more sophisticated form of heat flow equations such as the full heat flow transport equation may be needed for a more accurate comparison. The results obtained in the present study, however, give strong evidence that heat flow, or even higher-order moments, are able to reduce the sharp gradient features of the transport model profiles. This should be true regardless of the form of the heat flow equation being used.

Discussion and Conclusion

Closing the set of equations in the transport model by use of an heuristic heat flow expression, we have shown, as have *Demars and Schunk* [1992], that the transport and semikinetic models agree reasonably well up through the heat flow moments, in steady state with supersonic flow. However, for time-dependent situations, drastic disagreements occur, even for the lowest-order moments. One of the main differences between the two models is the development of shock fronts in the transport model. The semikinetic model produces smooth profiles in general, and the initial perturbation in the density and the other bulk parameters smooths out and diminishes in magnitude with time, returning rapidly to the steady state solution. Another difference between the results of the two models is that the correlation between the location of local maxima and minima seen in the results of the transport model are not seen in the semikinetic model. Additionally, the transport model may, under certain circumstances, develop various small scale features which are not seen in the semikinetic results. One of the main reasons for these differences is that the semikinetic model

properly includes the effects of velocity dispersion up through the higher velocity moments. It also includes the process of phase mixing, which is a thermal wave damping mechanism [*Palmadesso et al.*, 1988], which acts to smooth profiles and eliminate small-scale features.

In examining the general structure of various bulk parameters obtained by the two models, the fact that the semikinetic results are smoother as a result of velocity dispersion and phase mixing leads to the argument that the shocks seen in the transport model results are an artificial consequence of the lack of these processes in the transport model. Without the cross boundary relief that these two processes provide, the density, velocity and temperature of two adjacent regions can maintain very different values (i.e., a shock front). This view is supported by the fact that the results of the transport model are smoother when a higher heat flow is introduced artificially. One may argue that the discrepancies between the semikinetic and transport models may be due partly to the inability of equation (8) to properly describe the heat flow, and that therefore, the heat flow equations should be included in the transport model equation set. As discussed by *Palmadesso* [1988] and *Gombosi and Rasmussen* [1991], such a higher order model would still generate spurious waves since it lacks the higher moments needed to include full phase mixing. However, the solutions from such a model would differ somewhat from the transport model results presented in this paper, and might be closer to those of the semikinetic approach.

Much of the difference between the results of these two models is due to the fact that the transport model encounters difficulty in handling multi-streaming ion distributions. Although transport equations can be formulated to simulate multiple ion streams, this approach is useful only when the origin of the ion streams are known in advance. In many time-dependent situations, processes in the evolving system generate separate streams. The semikinetic model handles the development of these streams naturally.

One of the attractive features of the semikinetic model is that the additional information contained in the velocity distribution function makes it very easy to understand why certain features are seen in the bulk parameter profiles. For example, the increase in bulk velocity in a certain region is usually due to the presence of high-velocity ions, as in the plasma expansion into a low density region case, or due to the reduction of low-velocity ions as in the propagation of an ion depleted region case. On the other hand, the decrease of bulk velocity could be due to the presence of a second stream of low-velocity plasma, as in a density enhancement case, or the reduction of high-velocity ion as in the density cavity case. In the same way, the elevation of the ion temperature in various regions is often due to the presence of a second stream of ions and the depression of the temperature can be a consequence

of the narrowing of the velocity distribution in these regions or the presence of a dominant low temperature population.

Acknowledgments. This research is supported under NASA grant NAG8-134, NAG8-822, NAG8-239, NAGW-1554 and NGAW-2903.

The Editor thanks C. E. Rasmussen and another referee for their assistance in evaluating this paper.

References

Banks, P. M., and T. E. Holzer, The polar wind, *J. Geophys. Res.*, *73*, 6848, 1968.

Banks, P. M., and T. E. Holzer, Features of plasma transport in the upper atmosphere, *J. Geophys. Res.*, *74*, 6304, 1969.

Barakat, A. R., and R. W. Schunk, O^+ ions in the polar wind, *J. Geophys. Res.*, *88*, 7887, 1983.

Baugher, C. R., C. R. Chappell, J. L. Horwitz, E. G. Shelley, and D. T. Young, Initial thermal Plasma observation from ISEE 1, *Geophys. Res. Lett.*, 7, 657, 1980.

Boris, J. P., and D. L. Book, Solution of continuity equations by the method of flux-corrected transport, *Methods Comput. Phys.*, *16*, 85, 1976.

Brown, D. G., G. R. Wilson, and J. L. Horwitz, and D.L. Gallagher, 'Self-consistent' production of ion conics on return current region auroral field lines: A time-dependent, semi-kinetic model, *Geophys. Res. Lett.*, *18*, 1841, 1991.

Demars, H. G., and R. W. Schunk, Semikinetic and transport models of the polar and solar winds *J. Geophys. Res.*, *97*, 1581, 1992.

Dessler, A. J., and P. A. Cloutier, Discussion of letter by Peter M. Banks and Thomas E. Holzer, 'The polar wind,' *J. Geophys. Res.*, *74*, 3730, 1969.

Donahue, T. M., Polar ion flow: Wind or breeze?, *Rev. Geophys. Space Phys.*, *9*, 1, 1971.

Ganguli, S. B., and P. J. Palmadesso, Plasma transport in the auroral return current region, *J. Geophys. Res.*, *92*, 8673, 1987.

Ganguli, S. B., H. G. Mitchell, and P. J. Palmadesso, Behavior of ionized plasma in the high latitude topside ionosphere: The polar wind, *Planet. Space Sci. 35*, 703, 1987.

Gombosi, T. I., and A. F. Nagy, Time-dependent polar wind modeling, *Adv. Space Res.*, *8*, 59, 1988.

Gombosi, T. I., and C. E. Rasmussen, Transport of gyration dominated space plasmas of thermal origin, 1, Transport equations, *J. Geophys. Res.*, *96*, 7759, 1991.

Ho, C. W., J. L. Horwitz, N. Singh, T. E. Moore, and G. R. Wilson, Effects of magnetospheric electrons on polar plasma outflow: A semikinetic model, *J. Geophys. Res.*, *97*, 8425, 1992.

Ho, C. W., J. L. Horwitz, N. Singh, and G. R. Wilson, Comparison of transport and semikinetic model: prediction for evolution of a density enhancement in the polar wind, in *Physics of Space Plasmas (1992), SPI Conference Proceedings and Reprint Series, Number 12*, T. Chang, G. B. Crew, and J. R. Jasperse, eds. (Scientific Publishers, Cambridge, Mass., 1993), in press.

Holzer, T. E., J. A. Fedder, and P. M. Banks, A comparison of kinetic and hydrodynamic models of an expanding ion-exosphere, *J. Geophys. Res.*, *76*, 2453, 1971.

Horwitz, J. L., Parabolic heavy ion flow in the polar magnetosphere, *J. Geophys. Res.*, *92*, 175, 1987.

Horwitz, J. L., and C. R. Chappell, Observations of warm plasma in the dayside plasma trough at geosynchronus orbit, *J. Geophys. Res.*, *84*, 7075, 1979.

Horwitz, J. L., and M. Lockwood, The cleft ion fountain: A two-dimensional kinetic model, *J. Geophys. Res.*, *90*, 9749, 1985.
Hultqvist B., Extraction of ionospheric plasma by magnetospheric processes, *J. Atmos. Terr. Phys.*, *53*, 3, 1991.
Lemaire, J., and M. Scherer, Model of the polar ionexosphere, *Planet. Space Sci.*, *18*, 103, 1970.
Lemaire, J., and M. Scherer, Simple model of the polar ionexosphere in an open magnetic field, *Phys. Fluids*, *14*, 1683, 1971.
Li, P., G. R. Wilson, J. L. Horwitz, and T. E. Moore, Effect of mid-altitude ion heating on ion outflow at polar latitudes, *J. Geophys. Res.*, *93*, 9753, 1988.
Metzler, N., S. Cuperman, M. Dryer, and P. Rosenau, A time-dependent two-fluid model with thermal conduction for the solar wind, *Astrophys. J.*, *231*, 960, 1979.
Marubashi, K., Escape of the polar-ionospheric plasma into the magnetospheric tail, *Rep. Ionos. Space Res. Jap.*, *24*, 332, 1970.
Palmadesso P. J., S. B. Ganguli, and H. G. Mitchell, Jr., Multimoment fluid simulations of transport processes in the auroral zones, in *Modeling Magnetospheric Plasma*, *Geophys. Monogr. Ser.*, vol. 44, edited by T. E. Moore and J. H. Waite, p. 133, AGU, Washington, D. C., 1988.
Mitchell, H. G., and P. J. Palmadesso, A dynamic model for the auroral field line plasma in the presence of field-aligned current, *J. Geophys. Res.*, *88*, 2131, 1983.
Schunk, R. W., and D. S. Watkins, Electron temperature anisotropy in the polar wind, *J. Geophys. Res.*, *86*, 91, 1981.
Singh, N., Plasma perturbations created by transverse ion heating events in the magnetosphere, *J. Geophys. Res.*, *97*, 4235, 1992.
Singh, N., and R. W. Schunk, Numerical calculations relevant to the intial expansion of the polar wind, *J. Geophys. Res.*, *87*, 6487, 1982.
Singh, N., and R. W. Schunk, Temporal evolution of density perturbations in the polar wind, *J. Geophys. Res.*, *90*, 6487, 1985.
Singh, N., and R. W. Schunk, Ion acceleration in expanding ionospheric plasmas, in *Ion Acceleration in the Magnetosphere and Ionosphere*, *Geophys. Monogr. Ser.*, vol. 38, edited by T. Chang, p. 362, AGU, 1986.
Sonett, C. P., and D. S. Colburn, The SI^{+}-SI^{-} pair and interplanetary forward-reverse shock ensembles, *Planet. Space Sci.*, *13*, 675, 1965.
Wilson, G. R., C. W. Ho, J. L. Horwitz, N. Singh, and T. E. Moore, A new kinetic model for time-dependent polar plasma outflow: Initial results, *Geophys. Res. Lett.*, *17*, 263, 1990.

C. W. Ho, J. L. Horwitz, N. Singh, and G. R. Wilson, Department of Physics and Center for Space Plasma and Aeronomic Research, The University of Alabama in Huntsville, Huntsville, AL 35899.

(Received, August 3, 1992;
revised February 22, 1993;
accepted February 12, 1992)

Paper number 93JA00635.
0148-0227/93/93JA-00635$05.00

HO ET AL.: COMPARISON OF SEMIKINETIC AND TRANSPORT MODELS
HO ET AL.: COMPARISON OF SEMIKINETIC AND TRANSPORT MODELS
HO ET AL.: COMPARISON OF SEMIKINETIC AND TRANSPORT MODELS
HO ET AL.: COMPARISON OF SEMIKINETIC AND TRANSPORT MODELS
HO ET AL.: COMPARISON OF SEMIKINETIC AND TRANSPORT MODELS
HO ET AL.: COMPARISON OF SEMIKINETIC AND TRANSPORT MODELS
HO ET AL.: COMPARISON OF SEMIKINETIC AND TRANSPORT MODELS
HO ET AL.: COMPARISON OF SEMIKINETIC AND TRANSPORT MODELS
HO ET AL.: COMPARISON OF SEMIKINETIC AND TRANSPORT MODELS
HO ET AL.: COMPARISON OF SEMIKINETIC AND TRANSPORT MODELS
HO ET AL.: COMPARISON OF SEMIKINETIC AND TRANSPORT MODELS
HO ET AL.: COMPARISON OF SEMIKINETIC AND TRANSPORT MODELS
HO ET AL.: COMPARISON OF SEMIKINETIC AND TRANSPORT MODELS
HO ET AL.: COMPARISON OF SEMIKINETIC AND TRANSPORT MODELS
HO ET AL.: COMPARISON OF SEMIKINETIC AND TRANSPORT MODELS
HO ET AL.: COMPARISON OF SEMIKINETIC AND TRANSPORT MODELS
HO ET AL.: COMPARISON OF SEMIKINETIC AND TRANSPORT MODELS

Fig. 1. Comparison of the semikinetic and hydrodynamic steady state H^+ polar wind.

Fig. 2. Comparison of the time evolution of density, drift velocity, and parallel temperature for H^+ polar wind expansion into a low-density region, from the semikinetic and transport models. t_0 is the initial time, the next three profiles represent time t=5, 10, and 15 mins respectively.

Fig. 3. Distribution function for H^+ polar wind expansion into a low density region at (*a*) t=0 and (*b*) t=15 mins. The phase plot is in gray scale in which a darker shade represents a higher density.

Fig. 4. Comparison of density, drift velocity and parallel temperature of the (*a*) transport and (*b*) semikinetic model at t=15 mins for the case of H^+ polar wind expansion into a low-density region. Note that the transport model profiles have a one-to-one correspondence in their local minima and maxima.

Fig. 5. Comparison of the parallel heat flow of the semikinetic and transport model at t=15 mins for the case of H^+ polar wind expansion into a low-density region.

Fig. 6. Comparison of the time evolution of density, drift velocity and parallel temperature for a cold density enhancement in the H^+ polar wind from the semikinetic and transport models. The initial conditions for the drift velocity and parallel temperature in the transport model are calculated by using equations (10) and (11). The parallel temperature, according to the transport model, decreases at the location of the density enhancement, opposite to what occurs in the semikinetic model.

Fig. 7. Distribution function for a density enhancement in the H^+ polar wind at (*a*) t=0 and (*b*) t=15 mins. The phase plot is in gray scale in which a darker shade represents a higher density.

Fig. 8. Comparison of the time-evolution of density, drift velocity, and parallel temperature for a density cavity in the H^+ polar wind, from the semikinetic and transport models. Here t_0 is the initial time, the next three profiles represent time t=5, 10, and 15 minutes respectively.

Fig. 9. Distribution function of a density cavity in the H^+ polar wind at (*a*) t=0 and (*b*) t=15 mins. The phase plot is in gray scale in which a darker shade represents a higher density.

Fig. 10. Steady state H^+ polar wind parallel temperature for different heat flows. The dotted curve is the semikinetic model results and the other curves are obtained by using different values of $\eta_{\|}$ and $\eta_{\perp}$ (as indicated) in equations (8) of the transport model.

Fig. 11. Density and parallel temperature from the semikinetic model (dotted curve) and the transport model with $\eta_{\|}$ and $\eta_{\perp}$ given the value of 0 (dot-dashed curve), 1 (dashed curve), and 7.5 (solid curve). These profiles are for a density enhancement case at t=15 min.

Fig. 1. Comparison of the semikinetic and hydrodynamic steady state H^+ polar wind.

Fig. 2. Comparison of the time evolution of density, drift velocity, and parallel temperature for H^+ polar wind expansion into a low-density region, from the semikinetic and transport models. t_0 is the initial time, the next three profiles represent time t=5, 10, and 15 mins respectively.

Fig. 3. Distribution function for H^+ polar wind expansion into a low density region at (*a*) t=0 and (*b*) t=15 mins. The phase plot is in gray scale in which a darker shade represents a higher density.

Fig. 4. Comparison of density, drift velocity and parallel temperature of the (*a*) transport and (*b*) semikinetic model at t=15 mins for the case of H^+ polar wind expansion into a low-density region. Note that the transport model profiles have a one-to-one correspondence in their local minima and maxima.

Fig. 5. Comparison of the parallel heat flow of the semikinetic and transport model at t=15 mins for the case of H^+ polar wind expansion into a low-density region.

Fig. 6. Comparison of the time evolution of density, drift velocity and parallel temperature for a cold density enhancement in the H^+ polar wind from the semikinetic and transport models. The initial conditions for the drift velocity and parallel temperature in the transport model are calculated by using equations (10) and (11). The parallel temperature, according to the transport model, decreases at the location of the density enhancement, opposite to what occurs in the semikinetic model.

Fig. 7. Distribution function for a density enhancement in the H^+ polar wind at (*a*) t=0 and (*b*) t=15 mins. The phase plot is in gray scale in which a darker shade represents a higher density.

Fig. 8. Comparison of the time-evolution of density, drift velocity, and parallel temperature for a density cavity in the H^+ polar wind, from the semikinetic and transport models. Here t_0 is the initial time, the next three profiles represent time t=5, 10, and 15 minutes respectively.

Fig. 9. Distribution function of a density cavity in the H^+ polar wind at (*a*) t=0 and (*b*) t=15 mins. The phase plot is in gray scale in which a darker shade represents a higher density.

Fig. 10. Steady state H^+ polar wind parallel temperature for different heat flows. The dotted curve is the semikinetic model results and the other curves are obtained by using different values of $\eta_{\|}$ and $\eta_{\perp}$ (as indicated) in equations (8) of the transport model.

Fig. 11. Density and parallel temperature from the semikinetic model (dotted curve) and the transport model with $\eta_{\|}$ and $\eta_{\perp}$ given the value of 0 (dot-dashed curve), 1 (dashed curve), and 7.5 (solid curve). These profiles are for a density enhancement case at t=15 min.

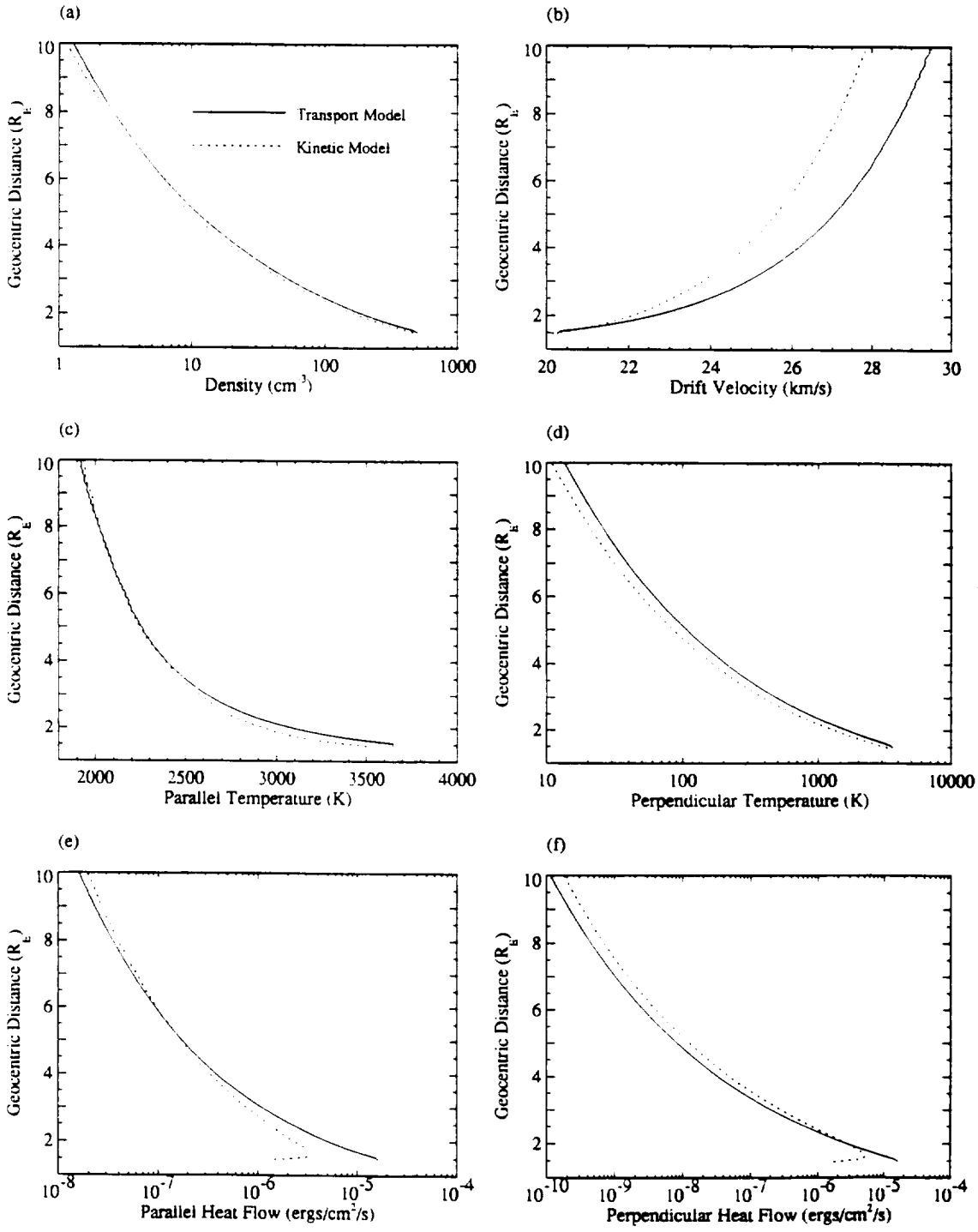
(a)
(b)
(c)
(d)
(e)
(f)
Transport Model
Kinetic Model
Geocentric Distance (R_E)
Density (cm^{-3})
Drift Velocity (km/s)
Parallel Temperature (K)
Perpendicular Temperature (K)
Parallel Heat Flow ($ergs/cm^2/s$)
Perpendicular Heat Flow ($ergs/cm^2/s$)

Figure 1

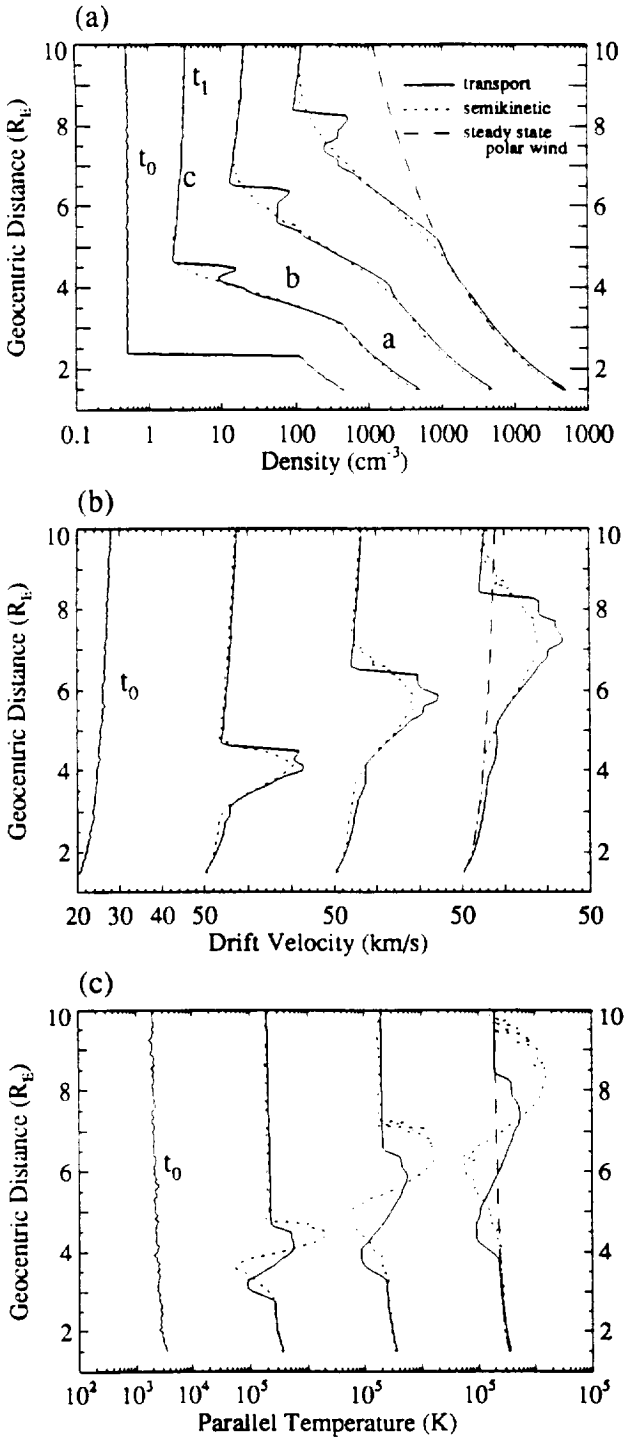
(a)
transport
semikinetic
steady state
polar wind
t_1
t_0
c
b
a
Geocentric Distance (R_E)
Density (cm^{-3})
0.1 1 10 100 1000 1000 1000 1000
(b)
t_0
Geocentric Distance (R_E)
Drift Velocity (km/s)
20 30 40 50 50 50 50
(c)
t_0
Geocentric Distance (R_E)
Parallel Temperature (K)
10^2 10^3 10^4 10^5 10^5 10^5 10^5

Figure 2

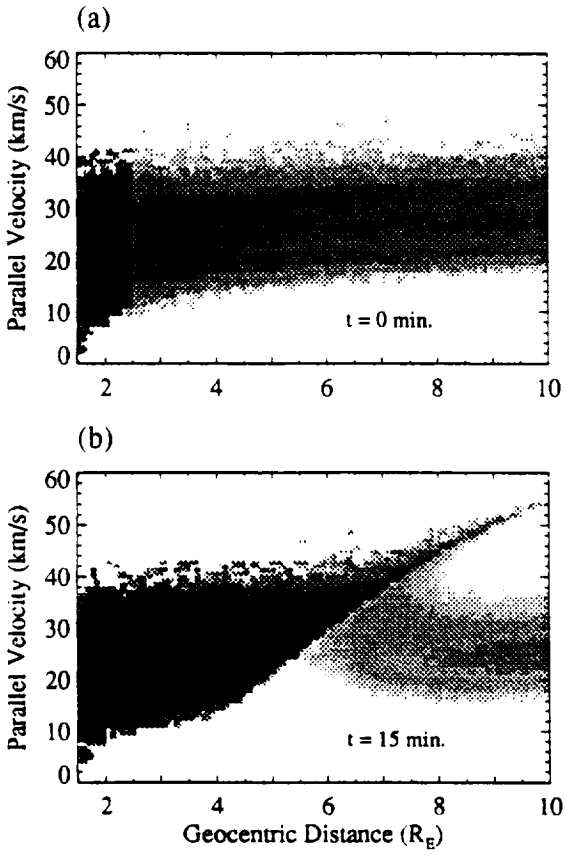
(a)
Parallel Velocity (km/s)
60
50
40
30
20
10
0
t = 0 min.
2
4
6
8
10
(b)
Parallel Velocity (km/s)
60
50
40
30
20
10
0
t = 15 min.
2
4
6
8
10
Geocentric Distance (R_E)

Figure 3

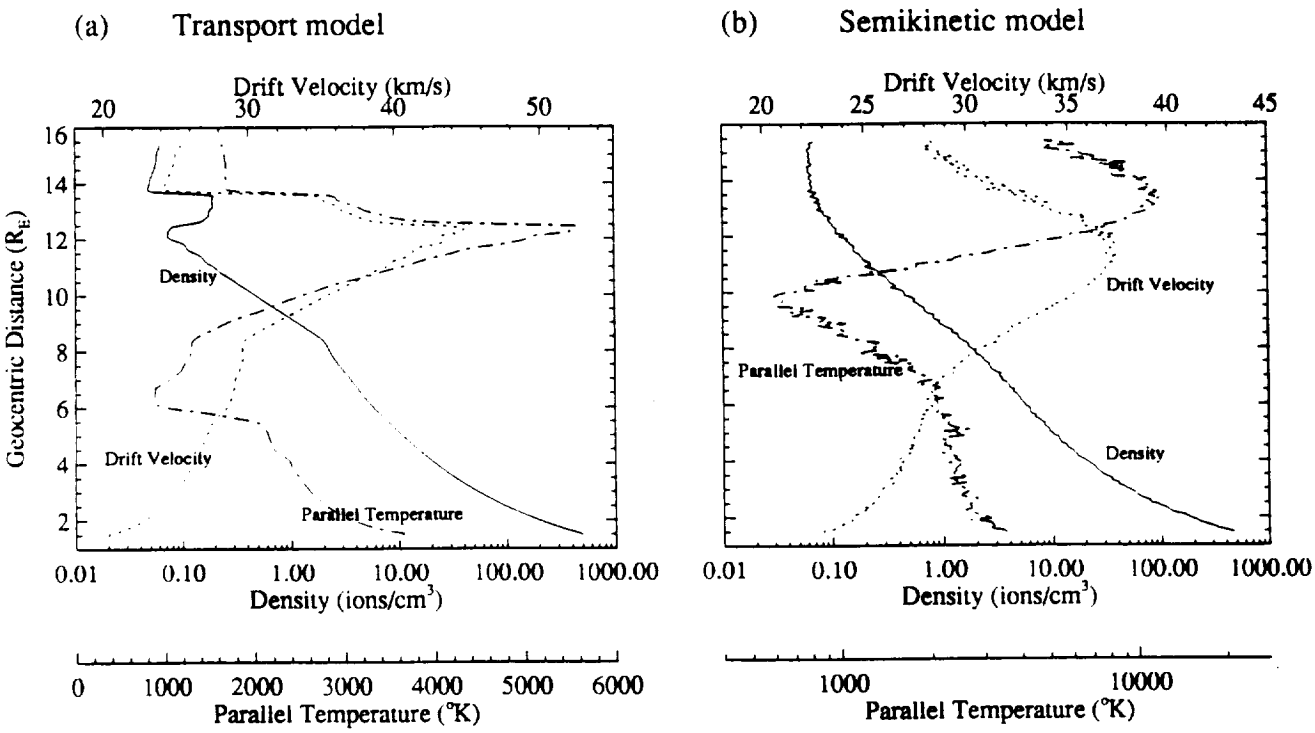
(a) Transport model
Drift Velocity (km/s)
20
30
40
50
16
14
12
10
8
6
4
2
Geocentric Distance (R_E)
Density
Drift Velocity
Parallel Temperature
0.01
0.10
1.00
10.00
100.00
1000.00
Density (ions/cm^3)
0
1000
2000
3000
4000
5000
6000
Parallel Temperature (°K)
(b) Semikinetic model
Drift Velocity (km/s)
20
25
30
35
40
45
Drift Velocity
Parallel Temperature
Density
0.01
0.10
1.00
10.00
100.00
1000.00
Density (ions/cm^3)
1000
10000
Parallel Temperature (°K)

Figure 4

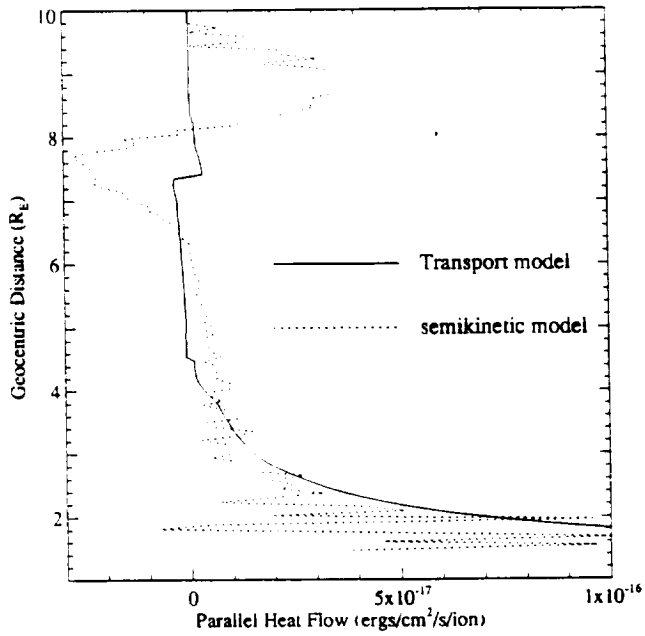
10
8
6
4
2
Geocentric Distance (R_E)
Transport model
semikinetic model
0
5x10^{-17}
1x10^{-16}
Parallel Heat Flow (ergs/cm^2/s/ion)

Figure 5

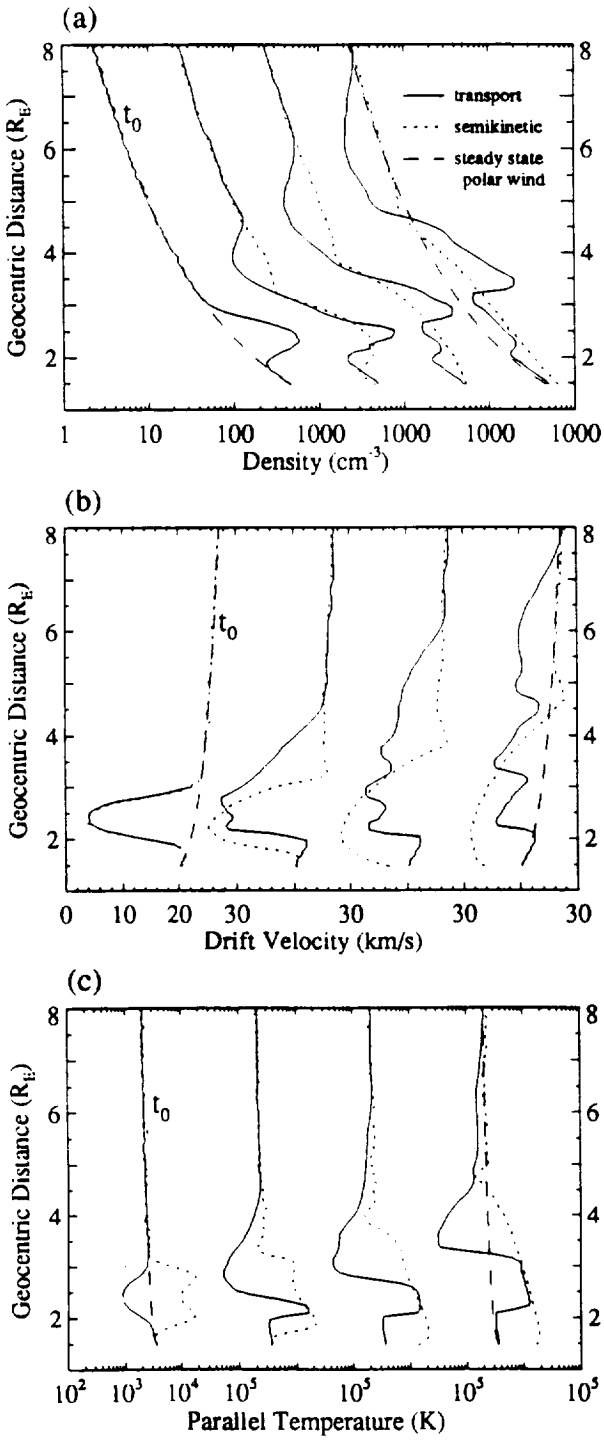
(a)
transport
semikinetic
steady state
polar wind
t_0
Geocentric Distance (R_E)
Density (cm^{-3})
(b)
t_0
Geocentric Distance (R_E)
Drift Velocity (km/s)
(c)
t_0
Geocentric Distance (R_E)
Parallel Temperature (K)

Figure 6

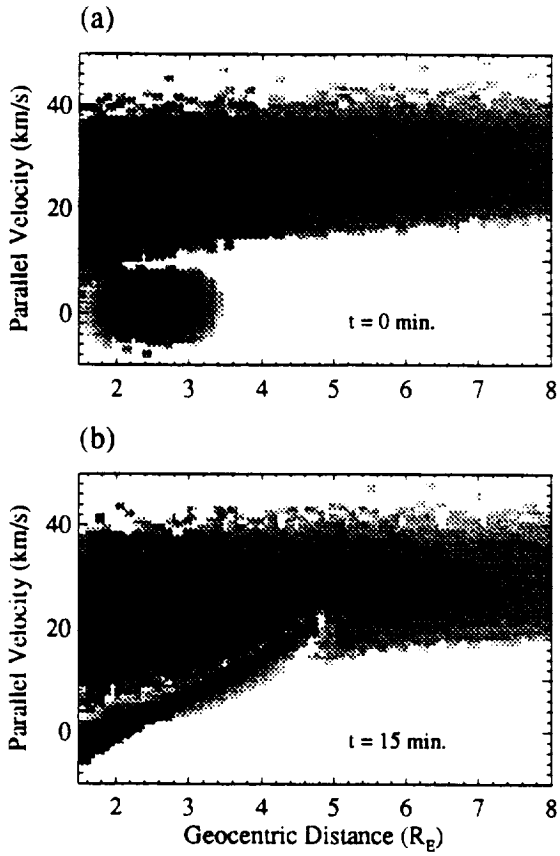
(a)
Parallel Velocity (km/s)
40
20
0
t = 0 min.
2
3
4
5
6
7
8
(b)
Parallel Velocity (km/s)
40
20
0
t = 15 min.
2
3
4
5
6
7
8
Geocentric Distance (R_E)

Figure 7

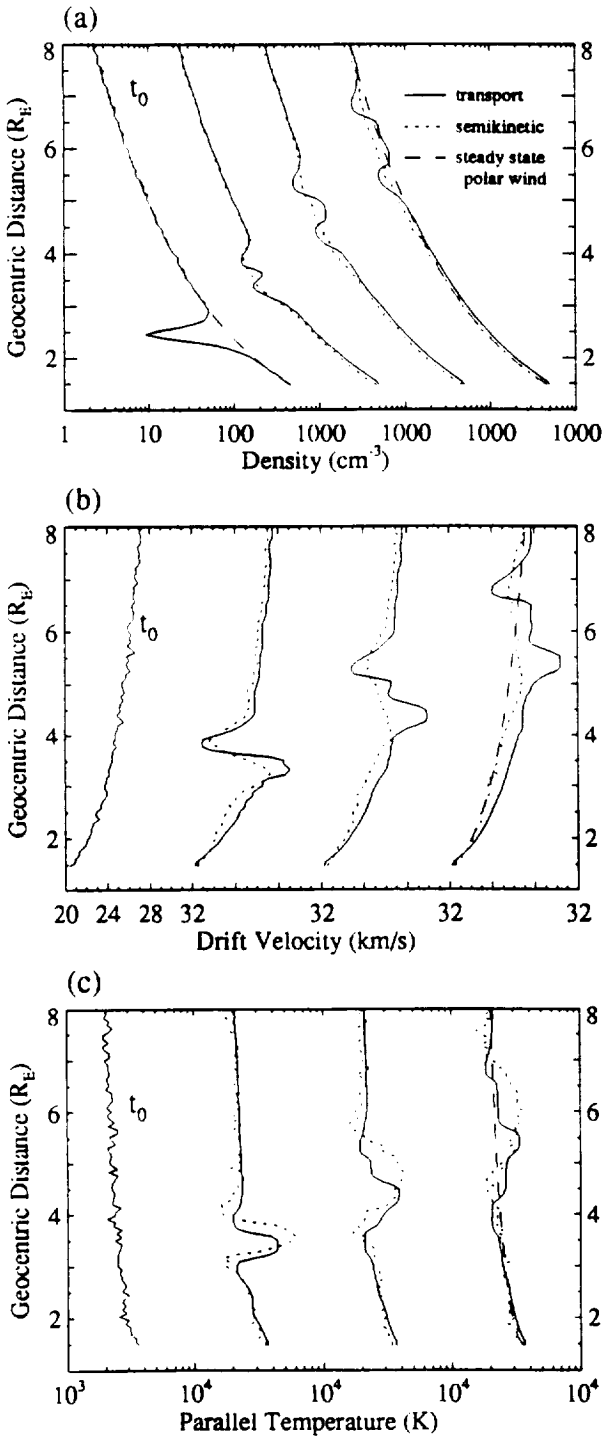
(a)
Geocentric Distance (R_E)
t_0
transport
semikinetic
steady state
polar wind
Density (cm^{-3})
(b)
Geocentric Distance (R_E)
t_0
Drift Velocity (km/s)
(c)
Geocentric Distance (R_E)
t_0
Parallel Temperature (K)

Figure 8

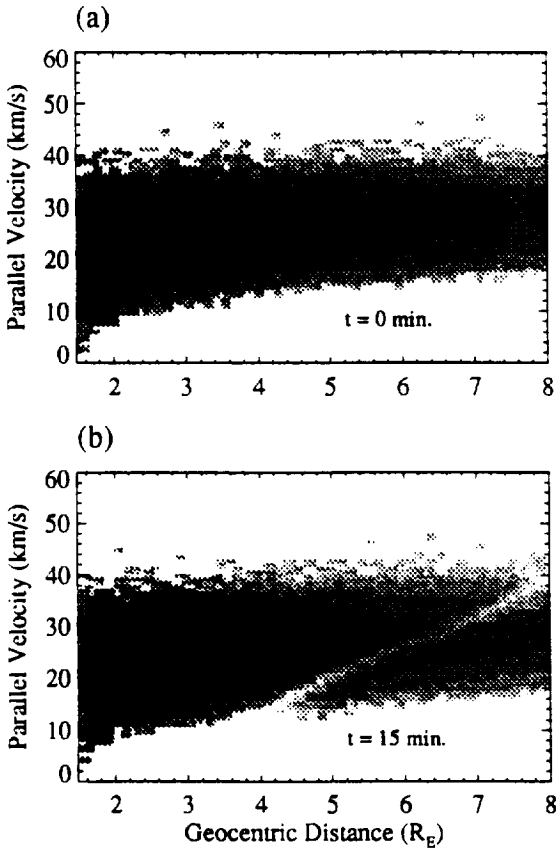
(a)
Parallel Velocity (km/s)
60
50
40
30
20
10
0
t = 0 min.
2
3
4
5
6
7
8
(b)
Parallel Velocity (km/s)
t = 15 min.
Geocentric Distance (R_E)

Figure 9

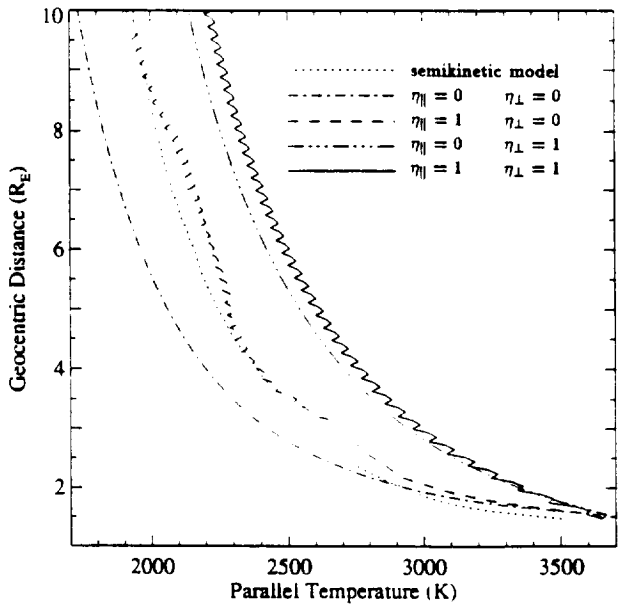
semikinetic model
$\eta_\parallel = 0$ $\eta_\perp = 0$
$\eta_\parallel = 1$ $\eta_\perp = 0$
$\eta_\parallel = 0$ $\eta_\perp = 1$
$\eta_\parallel = 1$ $\eta_\perp = 1$
Geocentric Distance (R_E)
Parallel Temperature (K)
10
8
6
4
2
2000
2500
3000
3500

Figure 10

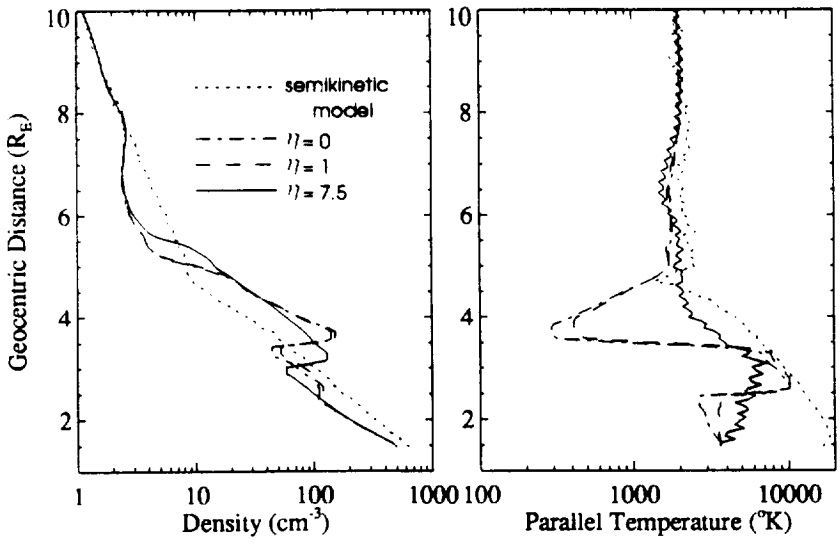
semikinetic model
η = 0
η = 1
η = 7.5
Geocentric Distance (R_E)
Density (cm^{-3})
Parallel Temperature (°K)
10
8
6
4
2
1
10
100
1000
100
1000
10000

Fig 11